Bulletin of Earthquake Engineering (2023) 21:4923–4950
https://doi.org/10.1007/s10518-023-01717-8

ORIGINAL ARTICLE

A risk-targeted approach for the seismic design of bridge piers

Francesca Turchetti[1] · Enrico Tubaldi[1] · John Douglas[1] · Mariano Angelo Zanini[2] · Andrea Dall'Asta[3]

Received: 21 March 2023 / Accepted: 4 June 2023 / Published online: 23 June 2023

Abstract

Designing a structure to resist earthquakes by targeting an explicit failure risk has been a key research topic over the past two decades. In this article, a risk-targeted design approach is developed for circular reinforced concrete bridge piers, based on a probabilistic optimization procedure aimed at minimising the design resisting moment at the pier base. In order to reduce the computational effort, a surrogate model is developed to describe the influence of two key design parameter (i.e., the pier diameter and the longitudinal reinforcement ratio) on the structural behaviour and performance. The proposed approach is applied in a case study for Italy for target mean annual frequencies of failure selected according to European codes using a probabilistic seismic hazard assessment for average spectral acceleration across a wide range of structural periods. The variation in the design parameters across Italy is considerable because of the large variation in seismic hazard. It is found that in areas of low seismic hazard the level of seismic design required is near the minimum allowed by Eurocode 8 in terms of reinforcement ratio. In areas of the highest seismic hazard much higher reinforcement ratios and pier diameters are required to meet the risk targets. If both pier diameter and longitudinal reinforcement ratios are considered as design parameters then the optimisation procedure may mean adjacent sites have significant different pairs of these parameters as the target can be reached in multiple ways. This problem can be solved by fixing one parameter and optimising the other.

Keywords Seismic design · Bridges · Risk-targeting · Seismic design maps · Earthquakes

✉ Francesca Turchetti
francesca.turchetti@strath.ac.uk

[1] Department of Civil and Environmental Engineering, University of Strathclyde, Glasgow, UK

[2] Department of Civil, Environmental and Architectural Engineering, University of Padova, Padua, Italy

[3] School of Architecture and Design, University of Camerino, Camerino, Italy

1 Introduction

The majority of seismic design codes used worldwide rely on force-based methods, where the earthquake action used for sizing the structural components of a system is expressed in the form of a Uniform Hazard Spectrum (UHS) (Gkimprixis et al. 2020; Shahnazaryan and O'Reilly 2021; Baltzopoulos et al. 2021). This provides, for a given location and a pre-defined return period T_R, the seismic demand, expressed in terms of spectral acceleration at different structural periods. The choice to design a structure in accordance with a "uniform" level of seismic demand relies on the assumption that such a procedure would lead to the same annual probability of failure (i.e. collapse) wherever the building is located (Gkimprixis et al. 2020; Silva et al. 2015). Various limit state conditions have to be considered, corresponding to UHS for different T_R values (e.g. 475 years for the ultimate limit state, which is the "benchmark" limit state in Eurocode 8 (CEN (2004a, b) EN 1998-1:2004)).

Following the development of modern performance-based earthquake engineering, the research community has focused on understanding whether such a design approach is able to ensure a sufficient and uniform level of structural safety against earthquake actions for different structures located at various sites. Many studies have shown that this objective was not achievable following a uniform hazard design framework (e.g. Cornell and Krawinkler 2000; Ellingwood 2008; Dall′ Asta et al.2016; Tubaldi et al. 2012). A recent Italian study within the RINTC Project (Iervolino et al. 2018) aimed at computing for some representative building archetypes and a series of sites across Italy the "implicit risk" characterizing code-compliant buildings. This study showed a strong hazard-dependency of the seismic safety of code-compliant buildings (Pacifico et al. 2022).

Over the past decade, risk-targeted seismic design emerged as one of the most promising approaches for designing structures with controlled seismic risk and/or loss levels. Various risk-targeted design methods have been developed and applied to solve a wide range of design problems (see e.g. Vamvatsikos and Aschheim 2016; Franchin et al. 2018; Žižmond and Dolšek 2019; Vamvatsikos et al. 2020; Barbato and Tubaldi 2013; Altieri et al. 2018; Dall'Asta et al. 2018; O'Reilly et al. 2022; Sinković et al. 2016; Rojas et al. 2011; Costa et al. 2010). Following the work of Luco et al. (2007), the principle of "risk-targeting" has been embedded in the development of design maps, which are currently used in US design codes (e.g. National Academies of Sciences, Engineering, and Medicine 2020; ASCE/SEI 7-10 2013). As discussed by Fajfar (2018), the risk-targeting paradigm and concepts of risk-targeted maps and behaviour factors (Žižmond and Dolšek 2019; Gkimprixis et al. 2019) are expected to form the basis of future design codes for many countries (Douglas and Gkimprixis 2018; Douglas and Ulrich 2013; Vanzi et al. 2015; Allen et al. 2015; Talebi et al. 2021).

While most of the studies and codes listed above focus on the design of buildings, risk-targeted bridge design is a less explored topic. In fact, only a few studies have proposed risk-targeting design methods for these structures. Wang et al. (2014) proposed a method to design reinforced concrete (RC) bridge columns to achieve a uniform risk of failure. The authors proposed a multi-parameter probabilistic seismic demand model to be further used in a uniform risk framework that was specifically developed, by identifying an appropriate target ductility, for the design of RC columns. The relationship between the failure probability of typical RC columns and ductility factors was analysed to define a method to identify the target ductility factor based on an acceptable failure probability for RC bridges located in different US regions. Zakeri and Zareian (2017) also developed a framework

based on full Monte Carlo probabilistic simulation within Probabilistic-Based Seismic Assessment (PBSA) while considering the correlation between demands in different components, to estimate bridge repair-cost ratios at various levels of column drift ratio. Based on this framework, these authors implemented Monte Carlo simulations and Bayesian updating to perform an extensive parametric analysis to estimate probabilities of collapse and the probabilities of exceeding a repair-cost ratio for various design-parameter configurations. These authors also find that column ductility demand μ_d, is not a reliable factor for risk-based design of bridges due to the high level of uncertainty in deriving μ_d. This finding is in contrast to those of Wang et al. (2014). More recently, Dang (2021) developed a direct risk-based seismic design approach for bridges based on incremental dynamic analysis, fragility and risk assessment, and life cycle cost analysis indicators, which are used as design input parameters to control the downtime due to the damage of key components such as rubber bearings.

Deb et al. (2022b) proposed a method for risk-targeted performance-based seismic design of bridge piers for Californian Ordinary Standard Bridges to facilitate risk-informed design and decision making. The proposed formulation has the advantage of finding a first physically realizable design point in the primary parameter space. This design point can be further refined by setting other bridge design variables to meet the requirements of capacity design, code-based minimum ductility capacity, minimum reinforcement, and/or other external restrictions and requirements, i.e. within a risk-targeted perspective. In a companion work, the same authors expanded the previously developed formulation to account for the aleatory uncertainty associated with the choice of finite element (FE) model parameters, and the epistemic uncertainty related to the use of finite datasets to estimate the parameters of the probability distributions characterizing the FE model and LS fragilities (Deb et al. 2022a). Lian et al. (2022) proposed the concept of seismic importance adjustment factor as a way to adjust the bridge seismic importance factor in seismic design codes, based on the evaluation of direct (i.e. repair costs) and indirect (i.e. increased travel time) losses. Hence, the seismic importance adjustment factor ensures the accomplishment of the target requirements in terms of seismic risk.

Additionally, the implementation of a rigorous and straightforward risk-targeted seismic design procedure helps achieve resilience of bridges against multiple hazards. A growing interest in Multi-Hazard Design (MHD) that accounts for cascading effects has been also developed in recent years, with studies dealing with the interaction between different hazards (Nikellis et al. 2019; Zaghi et al. 2016; Petrini et al. 2020) showing how the right balance between opposing design strategies can be found by adopting a "uniform-risk" strategy amongst different hazards.

The present study proposes a risk-targeted method for the seismic design of bridges. In particular, the proposed procedure addresses the design problem for RC piers in multi-span bridges. The only variables considered as free design parameters are the pier diameter and the longitudinal reinforcement ratio, which are the most important parameters that control the performance of a bridge pier designed according to capacity design principles. In order to reduce the computational effort, a metamodel is built to describe the changes in the bridge dynamic behaviour and seismic fragility with these two design parameters. The optimal values of the design parameters are found as the solution of a simplified reliability-based optimization problem aimed at minimising the pier resisting moment, without the need to resort to complex and time-consuming optimization strategies. The methodology is applied in various locations across Italy to illustrate the variations in the optimal risk-based design properties of bridges across regions with varying seismic hazard and soil conditions, and the impact of the choice of the target risk level on the design results.

The proposed procedure efficiently includes the seismic hazard at the construction site by developing a map for the design parameters for bridge piers required to obtain uniform risk over the territory. The present study is therefore the first attempt to deal with risk-targeting of bridge piers in Italy.

The rest of the paper is organised as follows. Section 2 illustrates the risk-targeted design procedure for bridge piers together with some design choices in the application of the procedure, Sect. 3 illustrates the case study and the results of the parametric study carried out to evaluate the fragility curves for different combinations of design parameters. Section 4 illustrates the application of the risk-targeted design procedure to selected sites characterised by different seismicity. In Sect. 5, risk-targeted design maps are developed for Italy, considering different design choices in terms of free design parameters, target risk levels, and soil type. In the final section, conclusions and future studies are outlined.

2 Risk-targeting design procedure

The next two sub-sections present the direct and inverse reliability problems corresponding to the assessment of the bridge risk and the design of the bridge properties that satisfy a predefined performance level. Similar to Wang et al. (2014) and Deb et al. (2022b), the risk-targeted design problem for a single bridge pier (such as that in Fig. 1) is considered. This simplification is introduced due to the role played by bridge piers in controlling the seismic behaviour of bridges and also to facilitate the illustration of the proposed risk-based design procedure.

2.1 Direct problem

The basis of the proposed design procedure is the solution of the direct reliability problem, which corresponds to evaluating the probability of exceeding one (or more) limit state(s) of interest during the time interval of interest. For this purpose, a cloud-based approach is

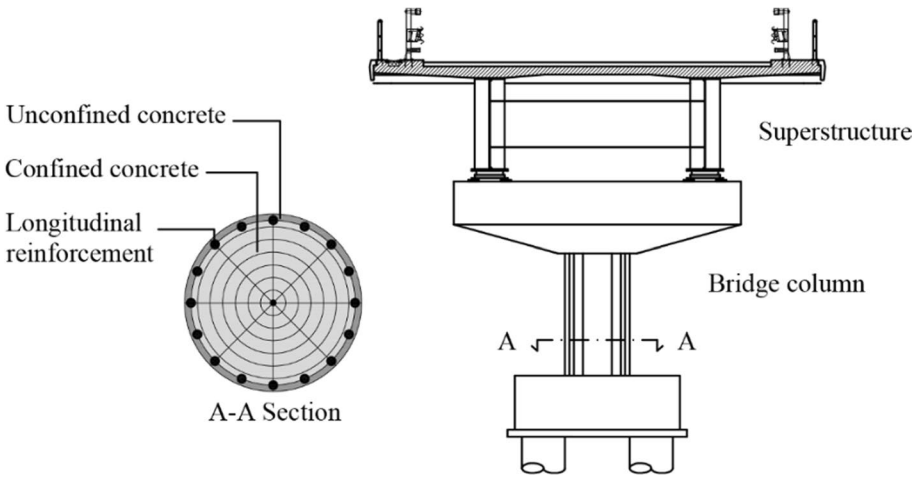

Fig. 1 Bridge model considered

employed (Jalayer et al. 2015), where the seismic input potentially causing the limit-state exceedance for the considered structural system and site is synthetically described by one (or more) random variable *IM*, whose realizations are positive real values *im*, and by a set of records that describe the variability of the earthquake characteristics (e.g. frequency content, duration) conditional to the *IM* value.

A capacity/demand format is used to evaluate the limit-state exceedance probability given the seismic intensity. This requires computing the probability of the demand exceeding the capacity conditional to the *IM* of the seismic input. The capacity is measured by a positive real-valued random variable C, whose possible realisations are denoted by c, with probability density function (PDF) $f_C(c)$ and cumulative density function (CDF) $F_C(c)$. The demand D is also expressed as a positive real valued random variable, whose possible realizations are denoted by d. The conditional distribution of the demand following events with a seismic intensity im is described by $f_{D|IM}(d|im)$. The probability of failure associated to the condition $C < D$ conditional to $IM = im$, is:

$$P_{f|IM}(im) = \int F_C(z) f_{D|IM}(z|im) dz \tag{1}$$

where z is a dummy variable.

With regards to the recursive properties of the seismic events during the time interval of interest, it is assumed that an event such that $IM > im$ can be described by a Poisson process fully defined by the Mean Annual Frequency (MAF) $v_{IM}(im)$. Under the assumptions that the probability distribution of the earthquake characteristics remains the same at each earthquake occurrence as does the probability of exceedance of the limit state, the failure events also follow a Poisson process and the MAF of failure can be evaluated as follows:

$$v_f = \int_{im} P_{f|IM}(im) \cdot \left| \mathrm{d}v_{IM}(im) \right| \tag{2}$$

The probability of failure in a time interval, e.g. the design lifetime t_L, can be obtained as:

$$P_{f,t_L} = 1 - e^{-v_f \cdot t_L} \tag{3}$$

In the following, it is assumed that the capacity is a log-normal random variable and the two parameters associated to this distribution, the median $\hat{c}$ and the standard deviation of the logarithms β_C, are known and independent of the seismic intensity. It is also assumed that the demand conditional on the seismic intensity is a log-normal random variable, with the parameters $\hat{d}$ and β_D denoting the median and standard deviation of the logarithms, respectively. The relationship between *IM* and D can be expressed as:

$$\log[D|IM = im] = \log\left[\hat{d}(im)\right] + \varepsilon = a + b \cdot \log(im) + \varepsilon \tag{4}$$

where ε is a normally distributed random variable with zero mean and standard deviation β_D. This model implies that only the median value varies with the intensity, while β_D is a constant. This approximation is generally satisfactory and widely adopted in seismic reliability problems, although it may lead to some inaccuracy in the performance assessment (e.g. Jalayer 2003; Gehl et al. 2015). The three parameters a, b and β_D can be determined through ordinary least squares regression, once an adequate number of *IM*-demand samples are known. The relationship expressed in Eq. (4) is herein assumed, but other closed-form

relations can be adopted, provided that they can be inverted (e.g. Romão et al. 2013). In this study, cloud analysis is carried out to develop the probabilistic seismic demand model (Jalayer 2003).

Under the above assumptions on the form of the capacity and of the demand, the conditional probability of failure can be expressed in a closed form as:

$$P_{f|IM}(im) = \Phi\left[\frac{\log\left[\hat{d}(IM)/\hat{c}\right]}{\sqrt{\beta_D^2 + \beta_C^2}}\right] \tag{5}$$

and the MAF of failure can be evaluated by Eq. (2) once the MAF of *im* is assigned.

If more than one failure mode is likely, then a system reliability analysis could be carried out to evaluate the failure probability of the bridge conditional to the *IM*, by also considering the correlation between the engineering demand parameters (EDPs) and based on the arrangement of the failure modes (e.g. series or parallel (Jalayer et al. 2007; Minnucci et al. 2022). The same considerations can be made in the case where multiple piers bridges are analysed.

2.2 Inverse problem

Let $\mathbf{x} \in \mathrm{R}^n$ denote the vector of design parameters (e.g. pier longitudinal reinforcement ratio and pier diameter). The risk-targeted design of bridges is an inverse reliability problem that can be cast in the form of an optimization problem: find the set of optimal design parameters $\mathbf{x}^*$ such that an objective function (cost function) is minimised. The solution must satisfy a stochastic constraint requiring that the failure probability (or the MAF of failure) is less or equal to a pre-fixed value, as well as other constraints on the values that can be assumed by $\mathbf{x}$. In mathematical terms, the problem can be formalised as follows:

$$\begin{aligned} \min_{\mathbf{x}} \quad & g(\mathbf{x}) \\ \text{subject to} \quad & \mathbf{h}(\mathbf{x}) \leq 0 \\ & v_f(\mathbf{x}) - \bar{v}_f \leq 0 \end{aligned} \tag{6}$$

where $g(\mathbf{x})$ is a cost function, depending on the design parameters, and $\mathbf{h}(\mathbf{x})$ is the set of constraints on the range of variation of $\mathbf{x}$. In Eq. (6), the dependency of the MAF of failure on the design parameters $\mathbf{x}$ has been made explicit. The choice of a suitable cost function is essential for ensuring that a single design point is obtained. In fact, various combinations of the design parameters ensure that $v_f(\mathbf{x}) - \bar{v}_f \leq 0$. Alternative formulations of the risk-based design problem for structures have been proposed (e.g. Franchin et al. 2018). It is noteworthy that under the assumption of failures following a Poisson process, targeting a level of the MAF of failure v_f is equivalent to targeting a level of failure probability in t_L years equal to $(1 - e^{-v_f * t_L})$.The optimization problem employed in this study does not require a complex algorithm. The problem is solved by first pre-mapping the values of cost function $g(\mathbf{x})$ across the domain of $\mathbf{x}$ using different techniques (simulation and interpolation, as described in the next sub-section), and then by using these gridded values to identify the optimal solution that complies with the target MAF.

2.3 Design procedure

The reliability-based design procedure for this problem consists of the following steps:

1. Select various combinations of the design parameters. These could be arranged to form a design of experiments matrix $\boldsymbol{X}_E = \left[\mathbf{x}_1 \ldots \mathbf{x}_j \ldots \mathbf{x}_{N_E} \right] \in R^{n \times N_E}$, where $\mathbf{x}_j = \left[x_{1j} \; x_{2j} \; x_{nj} \right]^T$ denotes the vector corresponding to the j-th combination of design parameters, and N_E denotes the total number of design points. In the following, a two-dimensional regular grid of possible design parameters (DPs) is considered as in Deb et al. (2022b). Alternatively, recourse can be made to Latin Hypercube Sampling, Sobol Sampling (e.g. Shekhar and Ghosh 2020; Hoang et al 2021) or alternative techniques;
2. For each combination of the DPs, the axial load value corresponding to the forces transmitted by the deck under the seismic load combination and the pier geometry is evaluated. This can be estimated using a linear FE model of the bridge. The design flexural resistance M_{Rd} of the plastic hinge section at the base of the pier is derived in accordance with Eurocode 8 provisions (CEN (2004a, b) EN 1998-1:2004), i.e., by considering appropriate safety factors for the capacity of concrete and steel. Subsequently, the transverse reinforcement is designed by applying capacity design principles to ensure that the pier fails under bending rather than shear and by satisfying the minimum requirements for confinement (CEN (2004a, b) EN 1998-1:2004); the confined concrete properties in the plastic hinge are evaluated using the Mander model (Mander et al. 1988) (see also Appendix E of CEN (CEN (2004a, b) EN 1998-1:2004) and a nonlinear FE model of the bridge is developed;
3. Cloud analysis is performed under a set of records representative of record-to-record variability effects to develop a probabilistic demand model for the EDPs of interest. In this study, a single limit state, corresponding to the exceedance of the displacement ductility capacity of the bridge, is considered. This is likely to be the most critical failure mode in newly designed bridges, because the application of capacity design principles ensures that the probability of occurrence of other failure modes (e.g. shear failure) is negligible;
4. Thus, the monitored EDP is the displacement demand at the pier top, which must be compared to the displacement capacity. This can be evaluated by performing a pushover analysis of the pier nonlinear model;
5. The probability $P_{f|IM}\left(im, \mathbf{x}_E\right)$ of exceedance of the limit state of interest conditional to the chosen IM and the combination of DPs in $\mathbf{x}_E$ is evaluated. In general, both the demand and the capacity are functions of $\mathbf{x}$. The use of a non-structure-specific IM is recommended to allow for comparison between fragility curves corresponding to different DP combinations. The only limit state we consider here is the exceedance of the pier displacement capacity, which is also a function of $\mathbf{x}$. This is the most critical failure mode, with other modes, such as shear failure or bearing failure, avoided due to the application of capacity design principles;
6. Based on the values of the conditional failure probability evaluated in correspondence of the support points, a surrogate model is fitted that provides the conditional failure probability for any possible value of $\mathbf{x}$ without needing to perform other seismic response analyses. The simplest approach for developing the surrogate model is to use linear interpolation. More sophisticated approaches could also be employed, such as those proposed by other authors for developing parametrized fragility functions (e.g. Shekhar and Ghosh 2020; Hoang et al 2021; Dukes et al. 2018; Franchini et al. 2022);

7. Given a site of interest, characterised by a hazard curve $v_{IM}(im)$, the MAF of failure given $\mathbf{x}$, $v_f(\boldsymbol{x})$, can be evaluated. This quantity is required for solving the problem formalised in Eq. (6). Obviously, the solution of the problem depends on the expression of the cost function and on the failure probability target (stochastic constraint), which are discussed below.

2.4 Cost function

The form adopted for the optimization problem is such that the consequences of pier failure in terms of direct and indirect losses are controlled by setting a maximum value of the MAF of failure. Since the total bridge life cycle cost is the sum of the cost of bridge construction and the cost due to failure, in order to minimise this cost one could consider the pier cost as the cost function. In order to avoid defining costs of the materials and of the construction, in the application illustrated in the next section, the cost function is assumed to coincide with the design resisting moment at the base of the pier, M_{Rd}. This quantity is expected to be correlated to the bridge construction cost, as it increases with the pier diameter, the amount of longitudinal reinforcement, the concrete class and other factors. Moreover, by minimising M_{Rd} the design shear (and thus the amount of transverse reinforcement) is also minimised and so are the forces transmitted to the foundations and to the deck.

2.5 Target failure probability

Fajfar (2018) discusses the difficulty in defining a target level of failure for structures because it is a reflection of personal and societal value judgements and experience in previous events. Therefore, there is no generally accepted target value. According to Eurocode 0 (CEN (2002) EN 1990:2002), the minimum recommended values of the reliability index for a reference period of 1 year should be 4.2 for consequence class CC1 structures (low consequences of failure), 4.7 for CC2 class structures (moderate consequences of failure), and 5.2 for CC3 class structures (high consequences of failure). These correspond respectively to a MAF of failure of 1.33×10^{-5} years^{-1}, 1.33×10^{-6} years^{-1}, and 9.96×10^{-8} years^{-1}. However, it is not clear whether the values recommended by Eurocode 0 should be considered for the seismic design, as the draft version of the revised Eurocode 0 explicitly exclude these (Fajfar 2018). Appendix F of the draft version of the revised Eurocode 8 (Dolsˇek et al. 2017) suggests a target of 2×10^{-4} years^{-1}, which according to Fajfar (2018) is a value comparable to the probabilities of failure estimated for buildings compliant with current seismic codes, also confirmed in a discussion among European code developers.

In Wang et al. (2014), a mean annual failure probability of 2.3×10^{-4} years^{-1} was considered for the risk-based design of reinforced concrete bridge piers. This value was chosen because it is the median among the values suggested in different American codes or standards (e.g. AASHTO 2010) for ultimate limit state (ULS) conditions. In Deb et al. (2022b), different values of the target MAF of failure are associated to the various failure modes considered: 1/225 years^{-1} for concrete cover crushing, 1/1000 years^{-1} for longitudinal bar buckling, and 1/2500 years^{-1} for longitudinal bar fracture. In Zanini and Hofer (2019) and Zanini et al. (2022) a 1-year target reliability value of 4.7 at ULS has been assumed for structural safety checks of common reinforced concrete arch bridges.

Douglas and Gkimprixis (2018) provide a summary of assessed and target MAFs of failure from the literature. Many studies have adopted the US target value of 2×10^{-4} without

much discussion, although Douglas et al. (2013) conclude that a target of 1×10^{-5} or even 1×10^{-6} would be easier to justify based on risk targets from other fields such as nuclear safety. Using a database of collapsed RC buildings in Italy and Greece over the previous few decades, Douglas and Gkimprixis (2018) conclude that the observed risk of collapse for such structures is between 1×10^{-6} and 1×10^{-5}. Because of the importance of road bridges both for life safety and their economic impact during and following earthquakes, a target MAF of failure of 1×10^{-6} is adopted for the following case study. The effect of this choice is examined by also considering 1×10^{-5} and 2×10^{-4} in subsequent steps.

3 Case study description and results of parametric analyses

A two-span bridge with a continuous multi-span deck is used to illustrate the application of the proposed risk-based design method. The bridge is representative of a class of medium-span bridges widely present in the European transport network (see Fig. 2). It was considered in previous studies by the same authors (e.g. Tubaldi et al 2013, 2022). The steel–concrete composite superstructure, designed according to Eurocode 4 (ECS) (CEN (2004a, b) EN 1994-1-1:2004), consists of an RC slab of width $B=12$ m, made with class C35/45 concrete (i.e., characteristic cylindrical compressive concrete strength of 35 MPa) and with grade B450C steel reinforcement bars (characteristic yield strength of 450 MPa), and of two steel girders placed 6 m apart, made of grade S355 steel (characteristic yield strength of 355 MPa). The distributed gravity load due to the deck's self-weight and non-structural elements is 138 kN/m, corresponding to a mass per unit length $m_d=14.07$ kg/m. The RC column is 5.4 m high and has a circular cross-section with diameter D_c. It is made of class C30/37 concrete. The deck is free to move in both the longitudinal and transverse directions at the abutments.

The three-dimensional FE model of the bridge is developed in OpenSees (2011) using the beam element with inelastic hinge developed by Scott and Fenves (2006) to describe the bottom of the pier, and linear elastic elements to describe the remaining part of the pier. The plastic hinge length is evaluated using the Eurocode 8 part 2 formula (CEN (2004a, b) EN 1998-1:2004). The geometric and material nonlinearities are accounted by means of the fibre-based section discretisation technique. This allows the representation of the influence of inelastic steel buckling and low cycle fatigue degradation. Degrading of stiffness in linear unloading/reloading is modelled according to Karsan and Jirsa (1969).The concrete stress–strain relationship is modelled through the Kent-Park model (Kent and Park 1971). The reinforcement steel is modelled by the Menegotto-Pinto constitutive model

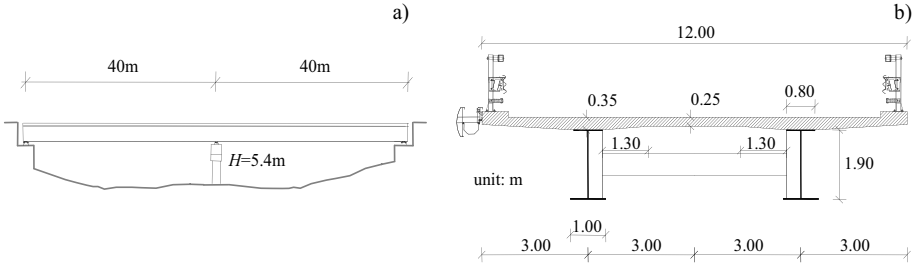

Fig. 2 **a** Two-span bridge profile, **b** transverse deck section. *Source* Tubaldi et al. (2013)

(Menegotto and Pinto 1973). The following material properties were assumed as fixed in all the models: a mean steel yield stress of f_{ym} = 517.5 MPa, maximum deformations of unconfined concrete under compression ε_{ccover} = 0.0035 and an ultimate steel deformation ε_{su} = 0.075. The material nonlinearity was described through a uniaxial material relationship for steel (tension and compression) and concrete (confined and unconfined). In this study, the Concrete02 model and the Steel02 model available in OpenSees (2011) were used: Concrete02, which is a linear tension softening material model that considers unloading stiffness degradation, was used to model the unconfined concrete in the cover and the confined concrete in the core of the pier, whereas Steel02 was used to model the reinforcement bars. The bearings were represented by zero length elements with a module of elasticity of 210,000 MPa connected to the elastic element via a rigid link-beam (both the translational and rotational degrees of freedom are constrained). The deck was not modelled but a vertical load was added to the column to simulate the weight of the deck. The elastic damping properties of the system are characterised by a Rayleigh damping model, with a 5% damping ratio assigned to the fundamental vibration modes in the longitudinal and transverse directions.

The same bridge is assumed to be located at various sites in Italy, characterised by different seismic hazards. A soil type A (corresponding to an time-averaged shear wave velocity up to 30 m depth of $V_{s,30}$ = 800 m/s) is considered for all the locations. Similarly to Deb et al. (2022b), the only DPs herein considered in the application of the risk-based design procedure are the pier diameter D_c and the longitudinal reinforcement ratio ρ_L,; thus $\mathbf{x}$ = [D_c, ρ_L]. It is noteworthy that these parameters are, among the many others that could be considered in $\mathbf{x}$, the ones that mostly affect the bridge's seismic performance (Wang et al. 2014; Deb et al. 2022b). These DPs are assumed to vary in a realistic range that reflects construction practice and satisfies code requirements. In particular, ρ_L can vary between 1 and 4%, whereas *Dc* can vary from 1.4 to 2.2 m. In order to develop the surrogate model for the bridge fragility, a regular grid of values of D_c and ρ_L is constructed. In particular, the values of D_c of 1.4 m, 1.8 m, and 2.2 m and the values of ρ_L of 1%, 2%, 3% and 4% are considered. For simplicity, two-dimensional linear interpolation is used to find the values of dependent variables corresponding to intermediate values of D_c and ρ_L. The various functions that are interpolated exhibit smooth and regular trends and, hence, more sophisticated interpolation methods or metamodeling techniques are not necessary.

Figure 3 shows the moment–curvature relationship for the section at the base of the pier for the different combinations of DPs investigated. The curves have been derived using a fiber-based discretisation of the cross section, considering different values of the axial force (to account for the effect of the pier's self-weight), as well as different levels of confinement, for the various values of D_c and ρ_L.

In all cases, the failure of the section corresponds to the crushing of the confined concrete, whereas the ultimate strain of the longitudinal reinforcement (assumed equal to 0.075) is never exceeded.

Figure 4 shows how the values of the design resisting moment M_{Rd} at the pier base (Fig. 4a) and the transverse reinforcement ratio ρ_S (Fig. 4b) increase with the diameter of the pier and the amount of longitudinal reinforcement. It can be noted that increasing D_c and ρ_L results in an increase of M_{Rd} and thus of ρ_S. The increase of ρ_S is due to the application of capacity design principles, with the design shear that increases with the base design resisting moment M_{Rd}. In general, the design resisting moment is more sensitive to D_c than to ρ_L for low D_c values. However, for high D_c values increasing ρ_L results in large increase of M_{Rd}. The transverse reinforcement ratio ρ_S varies between a minimum of 0.75% for low

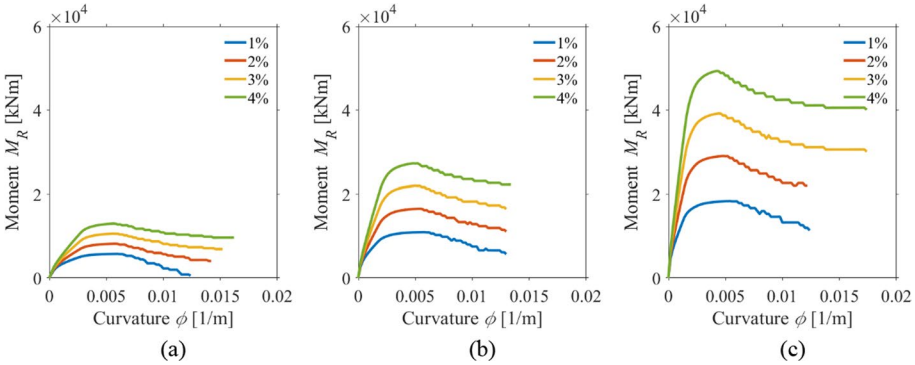

Fig. 3 Moment–curvature relationships for different combinations of DPs along the longitudinal direction **a** $D_c = 1.4$ m. **b** $D_c = 1.8$ m **c** $D_c = 2.2$ m

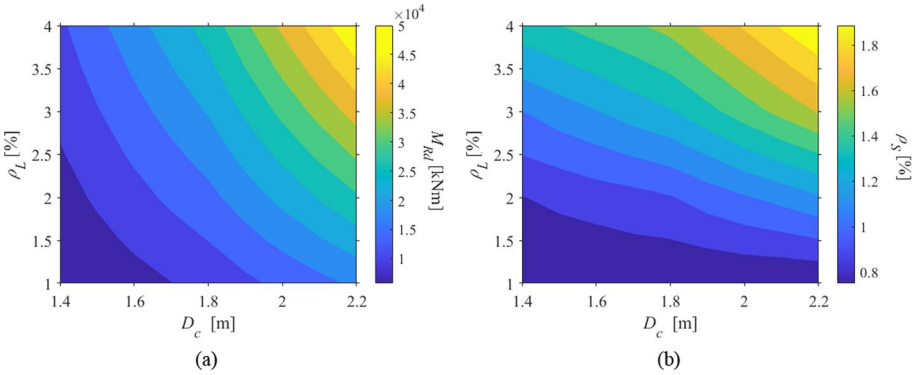

Fig. 4 **a** Design resisting moment M_{Rd} at the pier base and **b** transverse reinforcement ratio ρ_S for different combinations of the DPs

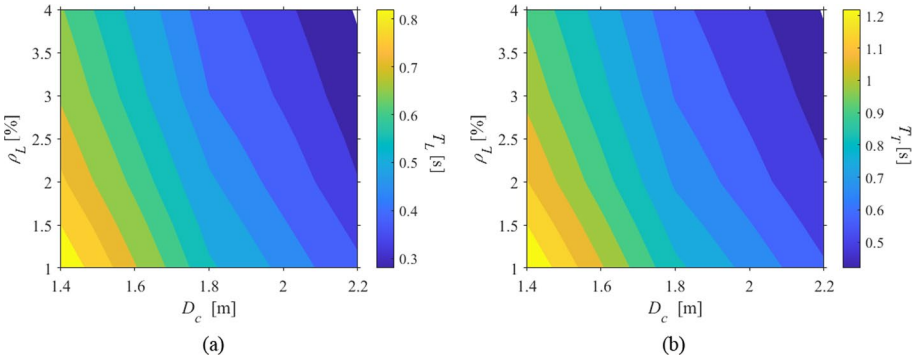

Fig. 5 Fundamental vibration periods T (in seconds) along the **a** longitudinal and **b** transverse direction for different combinations of DPs

values of D_c and ρ_L to a maximum of 1.89% for $D_c = 2.2$ m and $\rho_L = 4\%$. The diameter of the hoop bar ranges from 16 to 22 mm with a spacing between the bars from 80 to 35 mm.

Figure 5 shows the variation of the fundamental vibration periods along the longitudinal and transverse direction due to the variation of D_c and ρ_L. The longitudinal period is shorter than the transverse one due to the lower effective bending length. The bending lengths are equal to the pier height in the longitudinal direction, and the pier height plus the distance between the pier top and the deck centroid in the transverse one. In fact, the bearings placed at the bottom of the two girders in the steel–concrete composite deck result in transmission of bending moments from the deck to the pier under the transverse earthquake component. Both these periods reduce by increasing D_c and ρ_L as the structure becomes stiffer. In general, it can be observed that the quantities shown in Figs. 4 and 5 exhibit smooth trends with the design parameters.

Table 1 reports the values of the yield displacement d_y, the yield force V_y, and the ultimate displacements d_u for twelve combinations of DPs, in the longitudinal (L) and transverse (T) directions. The ultimate displacement has been identified based on a pushover analysis as the displacement that corresponds to the attainment of the ultimate curvature at the base section. The influence of higher order mode effects has been neglected in evaluating d_u, since they are not likely to affect the displacement demand significantly. Shear failure of the pier is not likely to occur thanks to application of capacity design principles.

The yield and ultimate displacements decrease with increasing diameter D_c, as expected (see e.g. Priestley et al. 2007). On the contrary, these quantities increase for increasing values of ρ_L. The increase of stiffness (and thus reduction of period) due to the increase of longitudinal reinforcement (i.e. flexural strength) is a typical feature of reinforced concrete sections, which is at the base of the development of direct-displacement based design criteria (see e.g. Priestley et al. 2007).

Cloud analysis is performed to develop the probabilistic seismic demand models (PSDMs) for the various design cases. For this purpose, the same ground motion records employed in Tubaldi et al. (2022) is used. This consists of 221 real records (120 of which taken from Baker et al. (2011)), which are representative of a wide range of conditions in terms of source-to-site distance (R) (from 8.71 to 126.9 km), soil characteristics (the time-average shear wave velocity in the top 30 m spans from 203 to 2016 m/s) and moment magnitude (M_w) (from 5.3 to 7.9). These records are not specific to any particular local site condition. The vertical component of the input is not considered.

Table 1 Values of yield displacement d_y, yield force V_y, and ultimate displacements d_u in longitudinal (L) and transverse (T) directions for different combinations of DPs

ρ_L	$D_c = 1.4$ m				$D_c = 1.8$ m				$D_c = 2.2$ m			
	1%	2%	3%	4%	1%	2%	3%	4%	1%	2%	3%	4%
$d_{y,L}$ [m]	0.036	0.039	0.041	0.043	0.027	0.030	0.032	0.033	0.022	0.024	0.026	0.027
$d_{u,L}$ [m]	0.167	0.164	0.175	0.191	0.141	0.155	0.166	0.171	0.138	0.149	0.163	0.168
$V_{y,L}$ [kN]	1520	2230	2950	3690	2780	4440	6080	7680	4710	7920	11,100	14,100
$d_{y,T}$ [m]	0.065	0.069	0.073	0.077	0.048	0.054	0.057	0.059	0.039	0.044	0.047	0.049
$d_{u,T}$ [m]	0.283	0.278	0.296	0.324	0.239	0.262	0.281	0.290	0.233	0.252	0.275	0.283
$V_{y,T}$ [kN]	1140	1670	2210	2760	2080	3320	4550	5750	3530	5930	8280	10,600

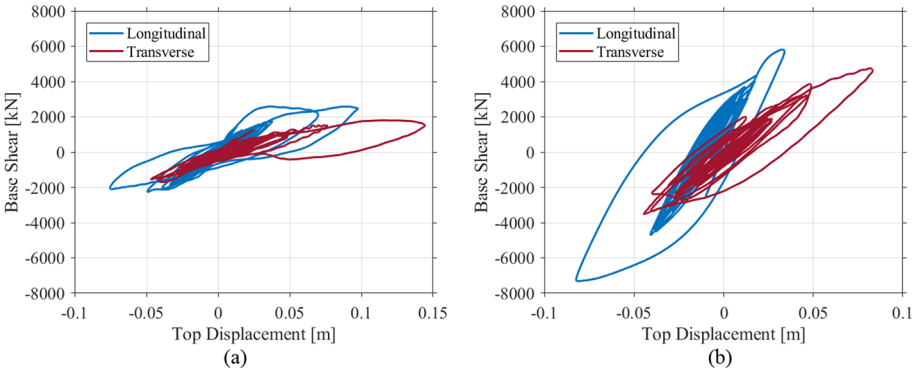

Fig. 6 Base shear-top displacement response along the two principal directions of the bridge for $D_c = 1.8$ m, and **a** $\rho_L = 1\%$ and **b** $\rho_L = 4\%$

Figure 6 shows the hysteretic response of the pier to a bi-directional ground-motion record, in terms of base shear-top displacement along the two principal directions of the bridge, for two different combinations of the design parameters. The top displacement is the displacement of the deck centroid, which coincides with the pier top displacement only in the case of longitudinal response. First of all, it can be observed that the response in the longitudinal direction is stiffer than in the transverse one. This is because the deck girders rest on two bearings, such that the effective length of flexure is larger for the transverse direction than for the longitudinal one. Moreover, the pier with higher longitudinal reinforcement is stiffer and stronger than the other one. This is also expected, given the higher bending moment capacity of the base section. Increasing the pier diameter while keeping the same amount of reinforcement ratio is also expected to increase the stiffness and strength of the system.

The maximum top displacements $u_{max,L}$ and $u_{max,T}$ along the longitudinal and transverse direction are considered to develop the PSDM and to evaluate the bridge performance. The intensity measure considered is $RotD50Sa_{avg}$, which is obtained as follows: first, the *RotD50* (Boore 2010) of the pseudo-acceleration response spectrum for the 221 records (two horizontal components) is computed, for a series of periods in the range between 0.1 s and 2.5 s, and for a 5% damping ratio. Then, the geometric mean of these is evaluated to obtain the $RotD50Sa_{avg}$. It is noteworthy that the proposed *IM* is not structure-specific.

Figure 7 shows the sample values of the maximum top displacement versus $RotD50Sa_{avg}$ in the log–log plane corresponding to the DP combinations of [1.4, 1%] and [2.2, 4%] along the longitudinal and transverse directions. In the same figures, the median of the fitted PSDMs is also plotted. It can be observed that $\log(u_{max})$ follows a linear trend with the $\log(RotD50Sa_{avg})$ for each combination of DPs. Nevertheless, some scatter is observed, particularly for high values of ρ_L. The displacement ductility achieved from the considered GMs ranges between 4.2 and 6.2 along the longitudinal direction and between 4.0 and 5.9 along the transverse direction. Table 2 reports the PSDM parameters along with the log-normal standard deviation of the regression models, β_D. The low values of β_D reveal a satisfactory fit of the PSDM to the data. Since the logs of the maximum displacements along the two directions exhibit a negligible correlation and they are assumed to jointly follow a bivariate normal distribution, they can be treated independently.

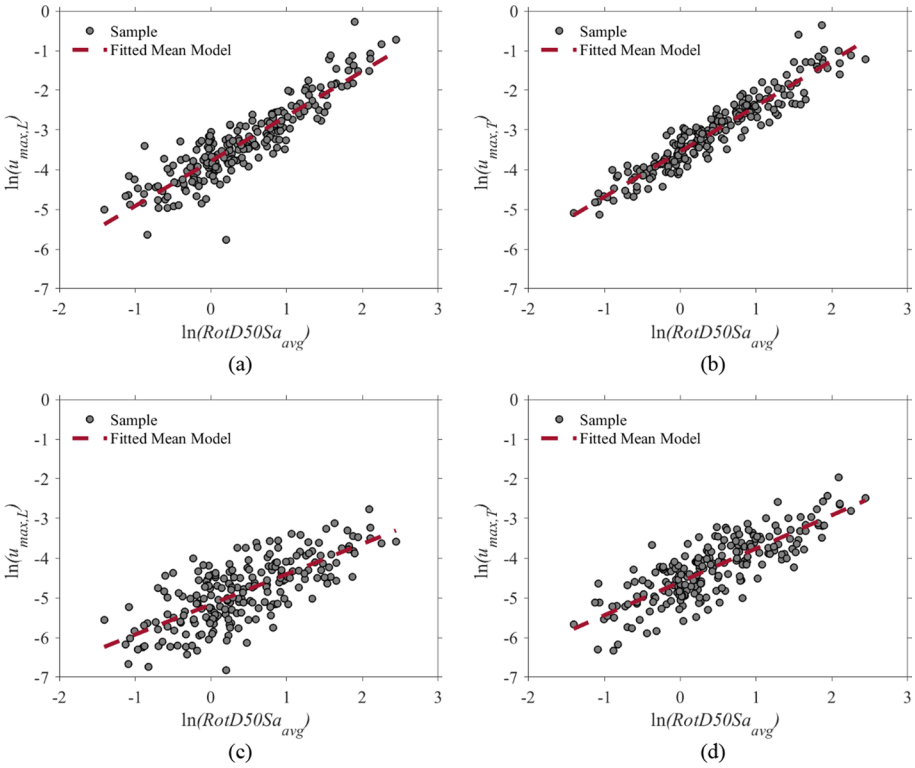

Fig. 7 Sample values and median model in terms of maximum top displacement for **a** $D_c = 1.4$ m and $\rho_L = 1\%$ in the longitudinal direction, **b** $D_c = 1.4$ m and $\rho_L = 1\%$ in the transverse direction, **c** $D_c = 2.2$ m and $\rho_L = 4\%$ in the longitudinal direction, **d** $D_c = 2.2$ m and $\rho_L = 4\%$ in transverse direction

Figure 8 reports the fragility curves for the various combinations of DPs. These have been constructed by evaluating, for each value of $RotD50Sa_{avg}$, the probability of the pier displacement demand along each of the two directions exceeding the corresponding displacement capacity (reported in Table 1). Equation (5) has been used to compute this probability. It is noteworthy that the capacity limits have been evaluated based on a pushover analysis, and no account is made of damage accumulation phenomena in the performance assessment, as e.g. done in Turchetti et al. (2023) with the use of the Ang-Park damage index. It can be observed that both the diameter and the longitudinal reinforcement ratio significantly affect the bridge fragility. Overall, increasing D_c is more effective than increasing ρ_L in reducing the bridge fragility. However, increasing the reinforcement ratio has a more significant effect in terms of reduction of fragility for large pier diameters than for low ones. These trends reflect the trend of variation of the resisting moment with D_c and ρ_L (see Fig. 4). Table 2 reports also the values of the median fragility capacity, $RotD50Sa_{avg,50\%}$, defined as the value of $RotD50Sa_{avg}$ corresponding to a probability of failure of 50%.

Table 2 Parameters of the regression models and values of lognormal standard deviation β_D

		$D_c = 1.4$ m				$D_c = 1.8$ m				$D_c = 2.2$ m			
	ρ_L	1%	2%	3%	4%	1%	2%	3%	4%	1%	2%	3%	4%
Long	log(*a*)	− 3.78	− 3.89	− 4.00	− 4.07	− 4.11	− 4.29	− 4.41	− 4.52	− 4.53	− 4.80	− 4.74	− 5.16
	b	1.13	1.10	1.07	1.04	1.09	0.98	0.90	0.85	1.00	0.89	0.76	0.76
	β_D	0.42	0.41	0.40	0.41	0.43	0.46	0.48	0.50	0.50	0.53	0.50	0.56
Transv	log(*a*)	− 3.54	− 3.62	− 3.68	− 3.76	− 3.91	− 4.04	− 4.12	− 4.20	− 4.21	− 4.40	− 4.24	− 4.60
	b	1.14	1.12	1.10	1.10	1.16	1.09	1.03	1.00	1.08	0.99	0.84	0.84
	β_D	0.30	0.30	0.31	0.31	0.33	0.36	036	0.37	0.38	0.39	0.40	0.45
	RotD50 $Sa_{avg,50\%}$	4.01	4.46	5.22	6.25	4.89	6.85	9.19	11.23	7.29	11.78	–	–

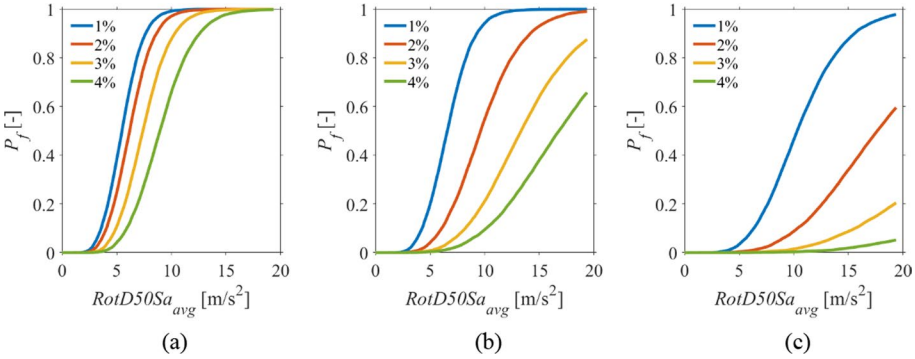

Fig. 8 Fragility curves for different combinations of DPs **a** $D_c = 1.4$ m **b** $D_c = 1.8$ m **c** $D_c = 2.2$ m

4 Results of the risk-targeting design approach for selected sites

Probabilistic seismic hazard assessment (PSHA) is carried out on a regular grid spaced by 0.05° for Italy. The same grid is used by the Italian National Institute of Geophysics and Volcanology (INGV) for developing hazard maps. The hazard curves for each site have been built using the software REASSESS V2.0 (Chioccarelli et al. 2019), using the ground motion prediction equation proposed by Lanzano et al. (2019) for *RotD50Sa*. The seismogenic source model is the one proposed by Meletti et al. (2008) with parameters taken from Barani et al. (2009). The interval of interest of the selected *IM* values ranges between 10^{-5} *g* and + 2 *g*, where *g* denotes acceleration due to gravity. The condition of "Soil Type A" (bedrock, i.e. vs30 ≥ 800 m/s) has been considered.

Figure 9a shows hazard curves in terms of MAF of exceedance of different values of $RotD50Sa_{avg}$ for three Italian cities: Milan (latitude 45.472N; longitude 9.177E), Naples (latitude 40.852N; longitude 14.268E), and L'Aquila (latitude 42.350N; longitude 13.400E). The three sites are exposed to roughly low-, mid-, and high-seismic hazard and have been considered in RINTC project to compare the risk levels across the country of various structures designed according to the Italian seismic codes (Tubaldi

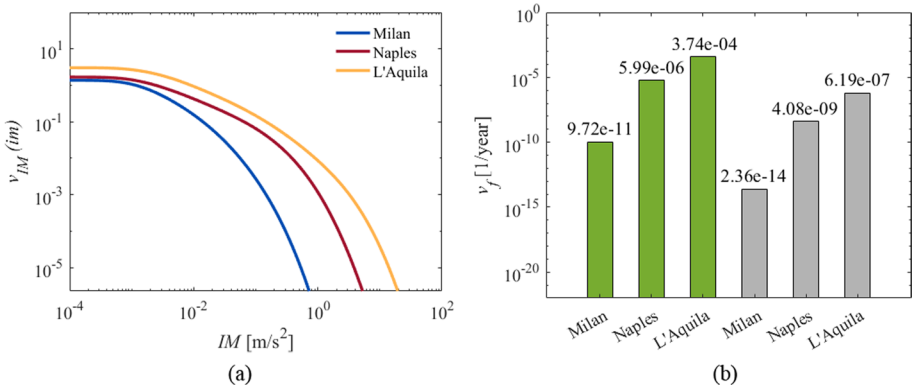

Fig. 9 **a** Comparison of hazard curves in terms of $IM = RotD50Sa_{avg}$ for three different sites in Italy; **b** comparisons of risks for $\rho_L = 1\%$, $D_c = 1.4$ m in green and $\rho_L = 4\%$, $D_c = 2.2$ m in grey

et al. 2012). Figure 9b compares the MAFs of bridge pier failure corresponding to the minimum values of DPs ($\rho_L = 1\%$, $D_c = 1.4$ m, in green), and to the maximum values of DPs ($\rho_L = 4\%$, $D_c = 2.2$ m, in grey) for the three considered sites. The MAF of failure for L'Aquila is very high for the minimum values of DPs, and it reduces by three orders of magnitude if the maximum values of DPs are considered; likewise, the MAF for Naples reduces from 6×10^{-6} to 4×10^{-9}. The MAF of failure for Milan is very low even for the minimum DPs, and it reduces by almost four orders of magnitude by considering the maximum values of DPs.

Figure 10a shows the mean annual frequency of pier failure for different combinations of DPs for the bridge located in L'Aquila. The optimal DP satisfying the stochastic constraint of a MAF of failure equal or less than 10^{-6} is also plotted in the figure and denoted by a star. Specifically, the star denotes a MAF of failure equal to 6×10^{-7}. The combinations of DPs have been evaluated by assuming discrete values for D_c and ρ_L, with an interval of 0.1 m for D_c, and of 0.005 for ρ_L. These intervals can be easily refined as there is no need to perform any further analysis. It can be observed that only one DP combination satisfies the required stochastic constraint in L'Aquila, which corresponds to a value of the resisting moment M_{Rd}, plotted in Fig. 4a (and replotted in Fig. 10b for convenience). Thus, it is possible to identify a point that minimises M_{Rd} (cost function) while satisfying the stochastic constraint. In the case of the bridge pier located in L'Aquila, the optimum DP corresponds to $D_c = 2.2$ m and $\rho_L = 0.04$ and a value of M_{Rd} of 49,330 kNm. Regarding the choice of the target MAF of failure equal or less than 10^{-6}, this value is close to the value of 1.33×10^{-6} that corresponds to consequence class CC2. Other values of the target MAF of failure are also considered in the next section.

Figure 11 shows the same results already shown in Fig. 10, but considering the bridge located in Naples rather than in L'Aquila. As expected, compared to L'Aquila there are more combinations of design parameters that satisfy the constraint on the acceptable risk of failure. Among these, the one that minimises the resisting moment corresponds to $D_c = 1.4$ m and $\rho_L = 3.5\%$. The identification of this point is straightforward, and does not require a complex optimisation algorithm but simply finding the combination that minimises M_{Rd} among the various pairs that satisfy the stochastic constraint. It is noteworthy that at mid-and high-seismic hazard sites, like Naples and L'Aquila, it is not

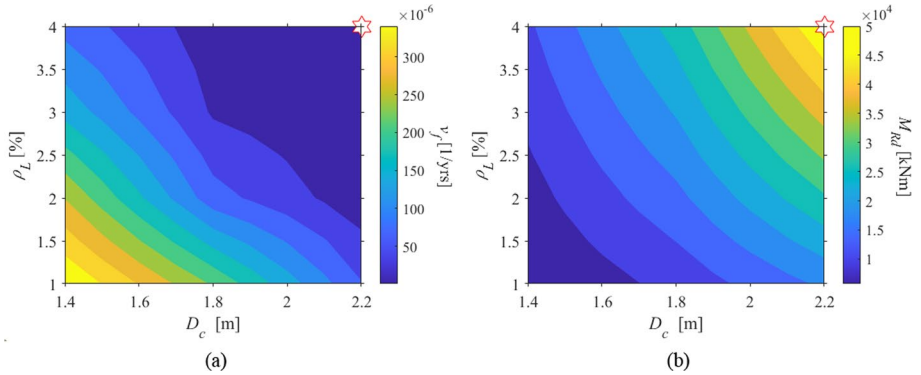

Fig. 10 **a** MAF of pier collapse for a bridge site in L'Aquila and **b** corresponding values of the resisting moment M_{Rd} (unit kNm) for different combinations of DPs. The optimal design point is marked by a star

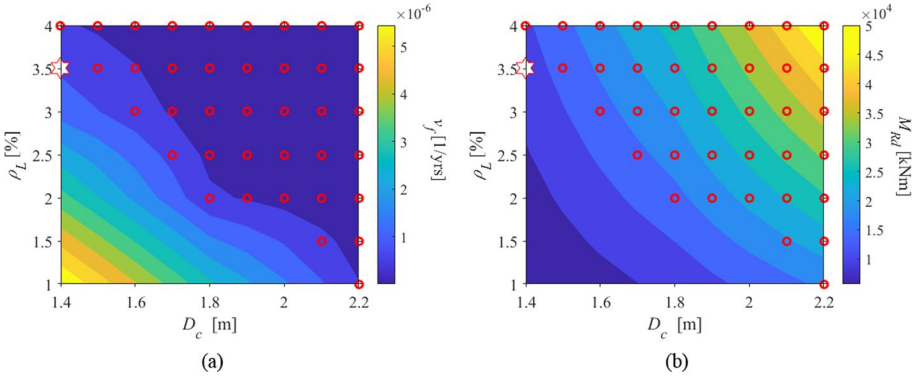

Fig. 11 **a** MAF of pier collapse and **b** corresponding values of the resisting moment M_{Rd} (unit kNm) for different combinations of DPs for a bridge site in Naples. The design parameters satisfying the stochastic constraint are marked with a circle, the optimal design point is marked by a star

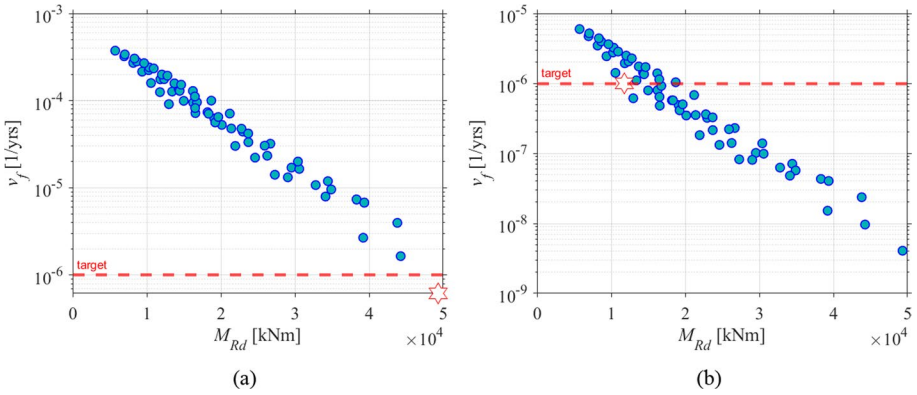

Fig. 12 Variation of the MAF of collapse vs. design resisting moment M_{Rd} obtained for various DP combinations for a bridge site in **a** L'Aquila and **b** Naples. The dashed red line indicates the target MAF of failure of 10^{-6} and the optimal design point is marked by a star. Note that the y-scale is different in the two plots

possible to achieve the target of 10^{-6} with the minimum reinforcement ratio ρ_L allowed by Eurocode 8.

Figure 12a shows the variation of the MAF of failure with the design resisting moment M_{Rd} for the site of L'Aquila. It can be observed that there is a strong and inverse correlation between these two quantities. A similar trend is observed for other sites. The case of Naples is illustrated in Fig. 12b.

5 Risk-based design maps for Italy

The proposed risk-based design procedure is applied to design the bridge pier across the whole of Italy, considering a target MAF of failure of 10^{-6}. The purpose of this analysis it to show how the designs would change across areas of different seismic hazard, and to

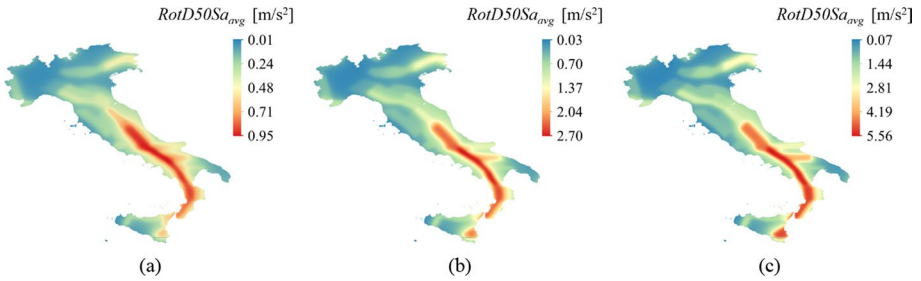

Fig. 13 Variation of $RotD50Sa_{avg}$ across Italy (unit m/s.^{2}) for return periods of 100 (**a**), 475 (**b**) and 2475 years (**c**)

evaluate differences between the regional distribution of the bridge design parameters and the regional distribution of seismic hazard.

Figure 13 shows the variation of $RotD50Sa_{avg}$ across Italy for return periods of 100 years, 475 years, and 2 475 years, corresponding respectively to 39%, 10%, and 2% probabilities of exceedance in 50 years. The intensity distribution across Italy is quite similar for the various return periods. However, for lower return periods higher intensities are observed in central Italy compared to southern Italy, whereas for the higher return period southern Italy shows intensities closer to those in central Italy. This is the effect of the different shape of the hazard curves for different locations, as already observed in Fig. 9a.

Figure 14 shows the variation of minimum resisting moment M_{Rd} at the base of the pier across Italy, corresponding to the optimal design point. In large parts of Italy the minimum value of M_{Rd}, corresponding to $\rho_L = 1\%$, $D_c = 1.4$ m, is sufficient to satisfy the constraint and achieve risk levels less than 10^{-6}. In these regions, the values of $RotD50Sa_{avg}$ for a return period of 475 years are less than about 0.1 m/s^2. In general, the contour plots of M_{Rd} follow a similar trend of $RotD50Sa_{avg}$, i.e., higher M_{Rd} values are required at sites of higher seismicity. The peak values of M_{Rd}, above 40 000 kNm, occur in parts of southern Italy, along the Apennine belt, and in the north-east, as expected.

Figure 15a and b show a map of the optimal values of the pier diameter D_c and of the longitudinal reinforcement ratio ρ_L. In regions with lowest seismicity, the optimal DPs coincide with the minimum values of D_c and ρ_L, whereas in the regions with highest seismicity, they coincide with the maximum ones, as expected. Non-smooth changes of

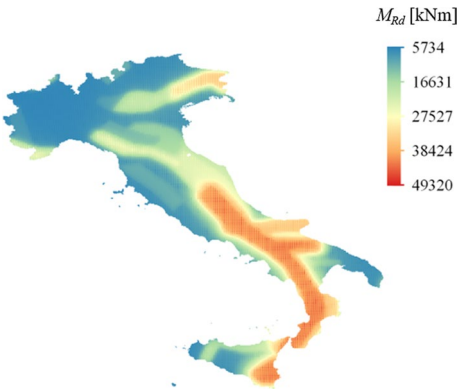

Fig. 14 Variation across Italy of the minimum resisting moment M_{Rd} at the base of the pier

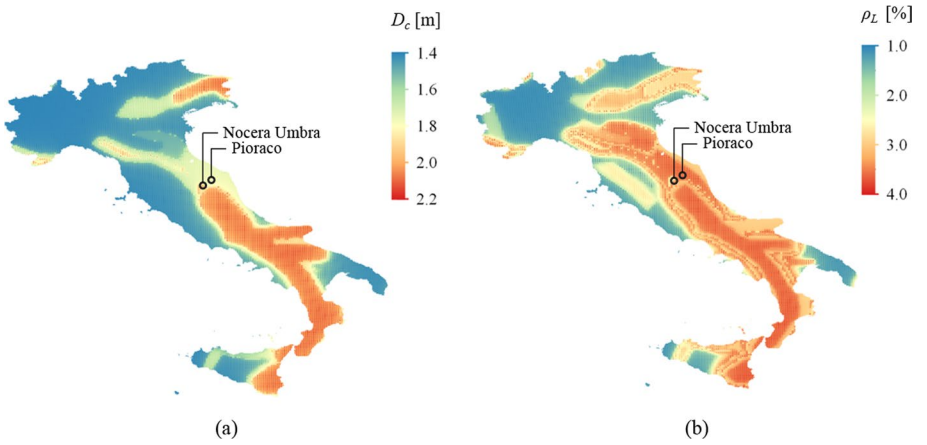

Fig. 15 Variation across Italy of the optimal pier diameter D_c (unit m) (**a**) and of the optimal ρ_L (expressed in terms of percentage) (**b**)

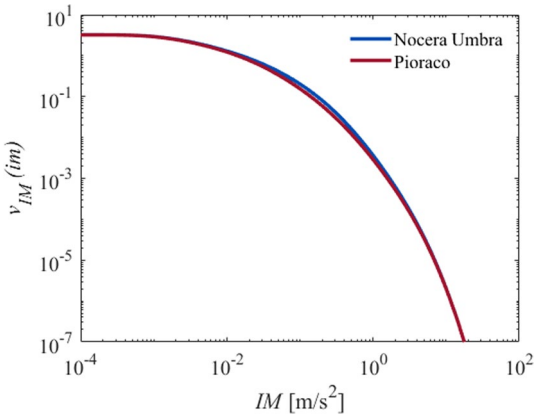

Fig. 16 Comparison of hazard curves in terms of $IM = RotD\text{-}50Sa_{avg}$ for the cities of Nocera Umbra and Pioraco

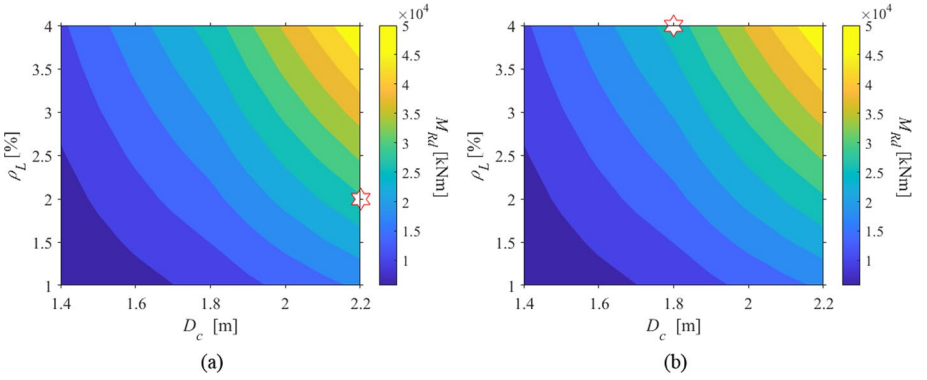

Fig. 17 Design resisting moment M_{Rd} at the pier base (in kNm) for different combinations of DPs for a bridge site in **a** Nocera Umbra and in **b** Pioraco. The optimal design point is marked by a star

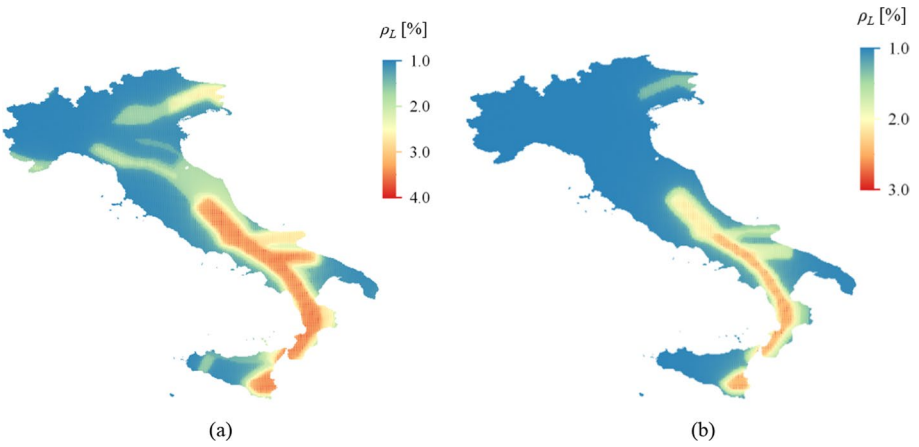

Fig. 18 Variation of the optimal ρ_L (expressed in terms of percentage) across Italy for $D_c = 2.2$ m obtained considering a target MAF of failure of 10^{-6} (**a**) and 10^{-5} (**b**)

optimal DP values can be observed across adjacent regions that are characterised by quite similar levels of hazard. This is because high values of D_c and low values of ρ_L yield similar risk levels to low values of D_c and higher values of ρ_L. For example, Nocera Umbra (latitude 43.114N; longitude 12.788E) and Pioraco (latitude 43.181N; longitude 12.974E) are two towns located closed to each other and with similar hazard levels (Fig. 16). Nevertheless, the optimal values of DPs are $D_c = 2.2$ m and $\rho_L = 2\%$ for the bridge in Nocera Umbra, and $D_c = 1.8$ m and $\rho_L = 4\%$ for the bridge in Pioraco, as shown in Fig. 17.

Obviously, a smoother variation of the optimal pier properties can be obtained if a single design parameter is considered, by keeping the other one fixed. Figure 18a shows the optimal values of ρ_L obtained considering a fixed diameter D_c of 2.2 m. In this case, ρ_L exhibits a smooth variation across the country. It is found that while $\rho_L = 4\%$ is necessary only in the high-hazard regions, it is sufficient to consider the minimum percentage of ρ_L in most of Italy.

The effect of the choice of the target risk level on the design parameters is evaluated by applying the proposed design procedure for a target MAF of failure of 10^{-5} and 2×10^{-4}. The results obtained considering a MAF of 10^{-5} for a fixed value of the pier diameter $D_c = 2.2$ m are shown in Fig. 18b. As expected, increasing the target risk level from 10^{-6} to 10^{-5} results in a significant reduction of the longitudinal reinforcement ratio across Italy. In this case, in many regions of Italy the minimum reinforcement amount according to Eurocode 8 is sufficient, and in the regions with high hazard the maximum value of ρ_L required is 3%.

The application of a MAF of failure of 2×10^{-4} is presented in Fig. 19. In this case, as shown in Fig. 19a, the highest value of the M_{Rd} is around 12,000 kNm, corresponding to a longitudinal reinforcement ratio ρ_L of 4% and $D_c = 1{,}4$ m. The minimum D_c is sufficient all over Italy while it is necessary to increase the amount of ρ_L in the southern regions with highest seismic hazard (Fig. 19b).

To provide insight into the effect of soil class on the application of the risk-targeting design procedure, the seismic hazard is assessed at the three sites previously considered (Milan, Naples and L'Aquila) for the soil types B, C and D. The new hazard

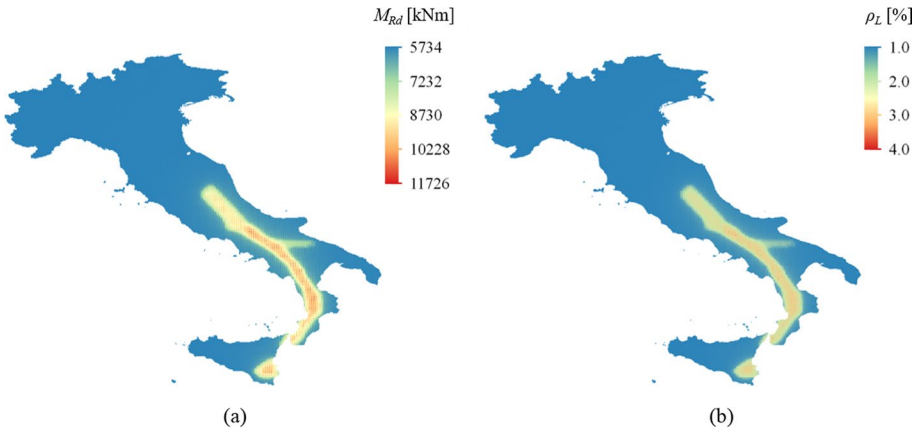

Fig. 19 Variation across Italy of the M_{Rd} at the base of the pier (**a**) and of the optimal ρ_L (expressed in terms of percentage) obtained considering a target MAF of failure of 2×10^{-4}

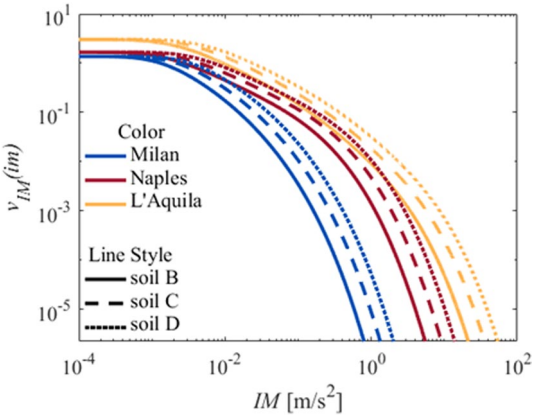

Fig. 20 Comparison of hazard curves in terms of $IM = RotD\text{-}50Sa_{avg}$ for three different sites in Italy assuming different soil classes

curves are obtained using the software REASSESS V2.1 (Chioccarelli et al. 2019) and using the same ground motion prediction equation adopted for soil type A. Figure 20 shows the new hazard curves for the three cities computed for soil B, C and D respectively whilst Table 3 reports the corresponding risk levels for two different combinations of design parameters. It can be observed that the increase of risk is highest for Milan and lowest for L'Aquila. Furthermore, the MAF of failure for the case of L'Aquila is above 10^{-6} even for the case of $\rho_L = 4\%$, $D_c = 2.2$ m and it is above 10^{-5} if soil D is considered. Thus, the soil type can have a considerable impact on the results of the risk-targeting design procedure.

Table 3 Risks computed for Milan, Naples and L'Aquila for two combinations of DPs ([1.4, 1%] and [2.2, 4%]) and for different soil classes

	Milan		Naples		L'Aquila	
	D_c = 1.4 m ρ_L = 1%	D_c = 2.2 m ρ_L = 4%	D_c = 1.4 m ρ_L = 1%	D_c = 2.2 m ρ_L = 4%	D_c = 1.4 m ρ_L = 1%	D_c = 2.2 m ρ_L = 4%
Soil B	4.75e-10	2.36e-13	1.39e-05	1.36e-08	6.26e-04	1.96e-06
Soil C	1.18e-08	7.79e-12	9.50e-05	1.19e-07	1.81e-03	8.59e-06
Soil D	1.25e-07	9.47e-11	3.67e-04	6.17e-07	3.77e-03	2.35e-05

6 Conclusions

This article illustrates a risk-targeting design procedure for bridge piers. The procedure identifies the optimal values of the pier diameter and longitudinal reinforcement ratio that minimise the resisting moment at the pier base while satisfying the stochastic constraint on the MAF of failure due to the exceedance of the pier displacement ductility capacity. The proposed procedure is based on the solution of a series of direct reliability problems where the pier seismic fragility is evaluated for different combinations of the design parameters, and using linear interpolation, which is justified by smooth variation of the interpolated quantities (e.g. fragility, risk, resisting moment of the base section) with the design parameters. The application of the proposed design procedure is illustrated by considering a two-span continuous bridge representative of medium-size bridges found widely in the European transport network. The bridge is assumed to be located in various sites in Italy, characterised by very different seismicity levels. Based on the obtained results, the following main conclusions can be drawn:

- The design resisting moment at the base of the pier exhibits a significant inverse correlation with the target MAF of failure and can be used to define the objective (cost) function to be minimised, as its value also affects the design of the transverse reinforcement of the pier, the design of the foundations, as well as the forces transmitted to the superstructure;
- Targeting values of the mean annual frequency of failure lower than 10^{-6} years^{-1} in regions of high seismicity requires design parameters (e.g. pier diameter) that are out of the investigated range, which represent realistic values for bridges in Italy that comply with the Eurocode 8 requirements (e.g. on the maximum and minimum value of the longitudinal reinforcement ratio);
- A large variation of the optimal design parameters is observed across Italy, as a result of significant variations in the seismic hazard.
- In large parts of Italy, the minimum longitudinal reinforcement according to Eurocode 8 is sufficient to guarantee a target mean annual frequency of failure below 10^{-5} years^{-1}. This latter value is significantly lower than the one considered in the US for risk-targeting, i.e. 2.3×10^{-4} years^{-1}.
- If both the pier diameter and the longitudinal reinforcement ratio are assumed as design parameters, non-smooth variations of the optimal values across adjacent sites could be obtained. This issue can be avoided by considering only a single design parameter and fixing the other.
- The site classification can influence the design results, especially in regions of high seismicity. Design maps should be built for different soil types to better estimate the effect of the site classification.

Future studies are required to evaluate the risk implicit to the design of bridge piers according to current seismic codes and to compare these results to the application of the proposed risk-based procedure. The proposed procedure can be extended to consider more design parameters than the ones considered here, as well as other possible failure modes related to different bridge components (e.g. bearings and abutments). It can also be applied to the risk-based design of other bridge types, including isolated bridges.

Funding The authors declare that no funds, grants, or other support were received during the preparation of this manuscript.

Declarations

Conflict of interest The authors have not disclosed any competing interests.

References

AASHTO (2010) AASHTO LRFD bridge design specifications. American Association of State Highway and Transportation Officials, Washington

Allen TI, Luco A, Halchuk S (2015) Exploring risk-targeted ground motions for the national building code of Canada. In: 11th Canadian conference on earthquake engineering, Victoria, BC

Altieri D, Tubaldi E, De Angelis M, Patelli E, Dall'Asta A (2018) Reliability-based optimal design of nonlinear viscous dampers for the seismic protection of structural systems. Bull Earthq Eng 16(2):963–982

ASCE (2013) Minimum design loads for buildings and other structures. ASCE/SEI 7–10

Baker JW, Lin T, Shahi SK, et al. (2011) New ground motion selection procedures and selected motions for the PEER transportation research program. In: PEER technical report 2011/03. Berkeley, Pacific Earthquake Engineering Research Center, University of California, Berkeley

Baltzopoulos G, Grella A, Iervolino I (2021) Seismic reliability implied by behavior-factor-based design. Earthq Eng Struct Dyn 50:4076–4096

Barani S, Spallarossa D, Bazzurro P (2009) Disaggregation of probabilistic ground-motion hazard in Italy. Bull Seismol Soc Am 99:2638–2661

Barbato M, Tubaldi E (2013) A probabilistic performance-based approach for mitigating the seismic pounding risk between adjacent buildings. Earthq Eng Struct Dyn 42(8):1203–1219

Boore DM (2010) Orientation-independent, nongeometric-mean measures of seismic intensity from two horizontal components of motion. Bull Seismol Soc Am 100(4):1830–1835

CEN (2002) EN 1990:2002 + A1 Eurocode—basis of structural design. European Committee for Standardization, Brussels

CEN (2004b) EN 1998–1:2004 Eurocode 8: design of structures for earthquake resistance—part 1: general rules, seismic actions and rules for buildings. European Committee for Standardization, Brussels

CEN (2004a) EN 1994–1–1:2004a Eurocode 4: design of composite steel and concrete structures. Part 2: composite bridges. European Committee for Standardization, Brussels

Chioccarelli E, Cito P, Iervolino I, Giorgio M (2019) REASSESS V2. 0: software for single-and multi-site probabilistic seismic hazard analysis. Bull Earthq Eng 17(4):1769–1793

Cornell CA, Krawinkler H (2000) Progress and challenges in seismic performance assessment. PEER Center News. https://apps.peer .berkeley.edu/news/2000spring/performance.html

Costa A, Romão X, Oliveira CS (2010) A methodology for the probabilistic assessment of behaviour factors. Bull Earthq Eng 8:47–64

Dall'Asta A, Dabiri H, Tondi E, Morici M (2018) Influence of time-dependent seismic hazard on structural design. Bull Earthq Eng 19:2505–2529

Dall′ Asta A, Tubaldi E, Ragni L (2016) Influence of the nonlinear behavior of viscous dampers on the seismic demand hazard of building frames. Earthq Eng Struct Dyn 45(1):149–169

Dang J. (2021) Seismic risk-based design of bridges. Reliability-based analysis and design of structures and infrastructures, Book Chapter 18, Edited by Ehsan Noroozinejad Farsangi, Mohammad Noori, Paolo Gardoni, Izuru Takewaki, Humberto Varum and Aleksandra Bogdanovic, CRC Press.
Deb A, Conte JP, Restrepo JI (2022a) Comprehensive treatment of uncertainties in risk-targeted performance-based seismic design and assessment of bridges. Earthq Eng Struct Dyn 51:3272–3295
Deb A, Zha AL, Caamaño-Withall ZA, Conte JP, Restrepo JI (2022b) Simplified risk-targeted performance-based seismic design method for ordinary standard bridges. J Bridg Eng 27(10):04022089
Dolsˇek M, ZˇizˇmondKosicˇSinkovicˊ JMN (2017) Simplified reliability-based verification format, working material for Annex F to revised EN 1998–1. University of Ljubljana, Ljubljana
Douglas J, Gkimprixis A (2018) Risk targeting in seismic design codes: the state of the art, outstanding issues and possible paths forward. Seism Hazard Risk Assess. https://doi.org/10.1007/978-3-319-74724-8_14
Douglas J, Ulrich T, Negulescu C (2013) Risk-targeted seismic design maps for mainland France. Nat Hazards 65:1999–2013
Dukes J, Mangalathu S, Padgett JE, DesRoches R (2018) Development of a bridge-specific fragility methodology to improve the seismic resilience of bridges. Earthq Struct 15(3):253–261
Ellingwood BR (2008) Structural reliability and performance-based engineering. Proc Inst Civ Eng Struct Build 161(4):199–207. https://doi.org/10.1680/stbu.2008.161.4.199
Fajfar P (2018) Analysis in seismic provisions for buildings: past, present and future. Bull Earthq Eng 16:2567–2608. https://doi.org/10.1007/s10518-017-0290-8
Franchin P, Petrini F, Mollaioli F (2018) Improved risk-targeted performance-based seismic design of reinforced concrete frame structures. Earthq Eng Struct Dyn 47(1):49–67
Franchini A, Sebastian W, D'Ayala D (2022) Surrogate-based fragility analysis and probabilistic optimisation of cable-stayed bridges subject to seismic loads. Eng Struct 256:113949
Gehl P, Douglas J, Seyedi DM (2015) Influence of the number of dynamic analyses on the accuracy of structural response estimates. Earthq Spectra 31(1):97–113
Gkimprixis A, Tubaldi E, Douglas J (2019) Comparison of methods to develop risk-targeted seismic design maps. Bull Earthq Eng 17(7):3727–3752
Gkimprixis A, Tubaldi E, Douglas J (2020) Evaluating alternative approaches for the seismic design of structures. Bull Earthq Eng 18(9):4331–4361
Hoang PH, Phan HN, Nguyen DT, Paolacci F (2021) Kriging metamodel-based seismic fragility analysis of single-bent reinforced concrete highway bridges. Buildings 11(6):238
Iervolino I, Spillatura A, Bazzurro P (2018) Seismic reliability of code-conforming italian buildings. J Earthq Eng 22:5–27
Jalayer F, De Risi R, Manfredi G (2015) Bayesian cloud analysis: efficient structural fragility assessment using linear regression. Bull Earthq Eng 13:1183–1203
Jalayer F, Franchin P, Pinto PE (2007) A scalar damage measure for seismic reliability analysis of RC frames. Earthq Eng Struct Dyn 36:2059–2079
Jalayer F (2003) Direct probabilistic seismic analysis: implementing nonlinear dynamic assessments. Stanford University, Stanford
Karsan ID, Jirsa JO (1969) Behavior of concrete under compressive loading. J Struct Div 95(12):2543–2563
Kent DC, Park R (1971) Flexural members with confined concrete. J Struct Eng-ASCE 97(7):1969–1990
Lanzano G, Luzi L, Pacor F, Felicetta C, Puglia R, Sgobba S, D'Amico M (2019) A revised ground-motion prediction model for shallow crustal earthquakes in Italy. Bull Seismol Soc Am 109:525–540
Lian Q, Yuan W, Guo J, Dang X (2022) Bridge seismic importance adjustment factor based on seismic risk. Soil Dyn Earthq Eng 160:107367
Luco N, Ellingwood BR, Hamburger RO, Hooper JD, Kimball JK, Kircher CA (2007) Risk-targeted versus current seismic design maps for the conterminous United States. In: Proceeding., SEAOC2007 Convention, Structural Engineers Association of California, Sacramento
Mander JB, Priestley MJN, Park RJ (1988) Theoretical stress–strain model for confined concrete. J Struct Eng 114(8):1804–1825
Meletti C, Galadini F, Valensise G, Stucchi M, Basili R, Barba S, Vannucci G, Boschi E (2008) A seismic source zone model for the seismic hazard assessment of the Italian territory. Tectonophysics 450:85–108
Menegotto M, Pinto PE (1973) Method for analysis of cyclically loaded reinforced concrete plane frames including changes in geometry and non-elastic behavior of elements under combined normal force and bending. In: Proceeding of IABSE Symposium, Lisbon, Portugal
Minnucci L, Scozzese F, Carbonari S, Gara F, Dall'Asta A (2022) Innovative fragility-based method for failure mechanisms and damage extension analysis of bridges. Infrastructures 7(9):122

National Academies of Sciences, Engineering, and Medicine (2020) proposed AASHTO guidelines for performance-based seismic bridge design. The National Academies Press, Washington. https://doi.org/10.17226/25913
Nikellis A, Sett K, Whittaker A (2019) Multi-hazard design and cost-benefit analysis of buildings with special moment-resisting steel frames. J Struct Eng 145:04019031. https://doi.org/10.1061/(ASCE)ST.1943-541X.0002298
OpenSees (2011) The open system for earthquake engineering simulation. Pacific Earthquake Engineering Research Centre, University of California, Berkeley
O'Reilly GJ, Yasumoto H, Suzuki Y, Calvi GM, Nakashima M (2022) Risk-based seismic design of base-isolated structures with single surface friction sliders. Earthq Eng Struct Dyn 51(10):2378–2398
Pacifico A, Chioccarelli E, Iervolino I (2022) Residential code-conforming structural seismic risk maps for Italy. Soil Dyn Earthq Eng 153:107104
Petrini F, Gkoumas K, Rossi C, Bontempi F (2020) Multi-hazard assessment of bridges in case of hazard chain: state of play and application to vehicle-pier collision followed by fire. Front Built Environ 6:580854
Priestley MJN, Calvi MC, Kowalsky MJ (2007) Displacement-based seismic design of structures. IUSS Press, Pavia, p 670
Rojas HA, Foley C, Pezeshk S (2011) Risk-based seismic design for optimal structural and nonstructural system performance. Earthq Spectra 27(3):857–880
Romão X, Delgado R, Costa A (2013) Alternative closed-form solutions for the mean rate of exceedance of structural limit states. Earthq Eng Struct Dyn 42:1827–1845
Scott M, Fenves G (2006) Plastic hinge integration methods for force-based beam-column. Elem J Struct Eng Asce 132(2):244–252
Shahnazaryan D, O'Reilly GJ (2021) Integrating expected loss and collapse risk in performance-based seismic design of structures. Bull Earthq Eng 19:987–1025
Shekhar S, Ghosh J (2020) A metamodeling based seismic life-cycle cost assessment framework for highway bridge structures. Reliab Eng Syst Saf 195:106724
Silva V, Crowley H, Bazzurro P (2015) Exploring risk-targeted hazard maps for Europe. Earthq Spectra 32:1165–1186
Sinković NL, Brozovič M, Dolšek M (2016) Risk-based seismic design for collapse safety. Earthq Eng Struct Dyn 45:1451–1471
Talebi M, Zare M, Farsangi EN, Soghrat MR, Maleki V, Esmaeili S (2021) Development of risk-targeted seismic hazard maps for the Iranian plateau. Soil Dyn Earthq Eng 141:106506
Tubaldi E, Dall'AstaDezi AL (2013) Reduced formulation for post-elastic seismic response of dual load path bridges. Eng Struct 51:178–187
Tubaldi E, Barbato M, Ghazizadeh S (2012) A probabilistic performance-based risk assessment approach for seismic pounding with efficient application to linear systems. Struct Saf 36:14–22
Tubaldi E, Ozer E, Douglas J, Gehl P (2022) Examining the contribution of near real-time data for rapid seismic loss assessment of structures. Struct Health Monit 21(1):118–137
Turchetti F, Tubaldi E, Patelli E et al (2023) Damage modelling of a bridge pier subjected to multiple earthquakes: a comparative study. Bull Earthq Eng. https://doi.org/10.1007/s10518-023-01678-y
Vamvatsikos D, Aschheim MA (2016) Performance-based seismic design via yield frequency spectra. Earthq Eng Struct Dyn 45:1759–1778
Vamvatsikos D, Bakalis K, Kohrangi M, Pyrza S, Castiglioni CA, Kanyilmaz A, Morelli F, Stratan A, D'Aniello M, Calado L, Proenca JM, Degee H, Hoffmeister B, Pinkawa M, Thanopoulus P, Vayas I (2020) A risk-consistent approach to determine EN1998 behaviour factors for lateral load resisting systems. Soil Dyn Earthq Eng 131:106008
Vanzi I, Marano GC, Monti G, Nuti C (2015) A synthetic formulation for the Italian seismic hazard and code implications for the seismic risk. Soil Dyn Earthq Eng 77:111–122
Wang Z, Padgett JE, Dueñas-Osorio L (2014) Toward a uniform seismic risk design of reinforced concrete bridges: a displacement-based approach. Struct Saf 50:103–112
Zaghi AE, Padgett JE, Bruneau M, Barbato M, Li Y, Mitrani-Reiser J, McBride A (2016) Forum paper: establishing common nomenclature, characterizing the problem, and identifying future opportunities in multi-hazard design. J Struct Eng (ASCE). https://doi.org/10.1061/(ASCE)ST.1943-541X.0001586,H2516001,142(12)
Zakeri B, Zareian F (2017) Bridge design framework for target seismic loss. J Bridg Eng 22(10):04017061
Zanini MA, Toska K, Feltrin G, Hofer L, Pellegrino C (2022) Seismic reliability assessment of an open-spandrel reinforced concrete arch bridge. In: Pellegrino C, Faleschini F, Zanini MA, Matos JC, Casas JR, Strauss A (eds) Proceedings of the 1st conference of the European association on quality control of

bridges and structures. EUROSTRUCT 2021. Lecture Notes in Civil Engineering, vol 200. Springer, Cham

Zanini MA, Hofer L (2019) Center and characteristic seismic reliability as new indexes for accounting uncertainties in seismic reliability analysis. Soil Dyn Earthq Eng 123:110–123

Žižmond J, Dolšek M (2019) Formulation of risk-targeted seismic action for the force-based seismic design of structures. Earthq Eng Struct Dynam 48(12):1406–1428